

**Zero- $\beta$  modeling of coaxial helicity injection in the HIT-II spherical torus**

**May 24, 2011**

R. A. Bayliss, C. R. Sovinec, and A. J. Redd

*Department of Engineering Physics, University of Wisconsin-Madison, 1500 Engineering Drive, Madison, Wisconsin 53706, USA.*

Prepared for submission to Physics of Plasmas

NOTICE

This report was prepared as an account of work sponsored by the United States Government. Neither the United States nor the United States Department of Energy, nor any of their employees, nor any of their contractors, subcontractors, or their employees, makes any warranty, expressed or implied, or assumes any legal liability or responsibility for the accuracy, completeness, or usefulness of any information, apparatus, product or process disclosed or represents that its use would not infringe privately owned rights.

Zero- $\beta$  modeling of coaxial helicity injection in the HIT-II spherical torus

R. A. Bayliss, C. R. Sovinec, and A. J. Redd

*Department of Engineering Physics, University of Wisconsin-Madison, 1500 Engineering Drive, Madison, Wisconsin 53706, USA.*

Coaxial helicity injection (CHI) in the HIT-II [Helicity Injected Torus, A. J. Redd, *et al.*, Phys. Plasmas **9**, 2006 (2002)] spherical torus is modeled with time-dependent resistive magnetohydrodynamics computations run to steady state for conditions without strong relaxation. Laboratory and computed results on injector current and plasma current agree reasonably well as toroidal magnetic field and injector flux are scaled. The scalings are consistent with a dimensional estimate from the Grad-Shafranov equation that provides a new perspective on a previously published model based on a current-sheet equilibrium and the magnetic pressure required for the ‘bubble-burst’ criterion. Numerical solutions of the Grad-Shafranov equation with an assumed current profile also indicate large qualitative changes as the predicted criterion is crossed.

PACS numbers: 52.55Wq, 52.55Fa, 52.65Kj

The strong curvature, shaping, and high normalized pressure ( $\beta$ ) of spherical torus (ST) plasmas lead to confinement and stability properties that are distinct from large aspect-ratio tokamaks. Driving plasma current also requires special consideration of the geometric limitations on passing time-dependent magnetic flux through a small central column. The coaxial helicity injection (CHI) method is a direct-current (DC) alternative<sup>1</sup> to conventional inductive loop voltage. CHI biases a pair of toroidally symmetric electrodes that intercept the strike points of open poloidal magnetic field to generate linked poloidal and toroidal magnetic flux. Maintaining an electrostatic bias on the ‘injector’ flux then sustains parallel current density in the presence of resistive dissipation. The CHI method was first tested for STs in the Helicity Injected Torus (HIT) and HIT-II experiments—as the sole source of current drive in the case of HIT and with transition to Ohmic drive in HIT-II.<sup>2,3</sup> When gradients of parallel current density are sufficient to excite symmetry-breaking MHD activity, magnetic relaxation<sup>4</sup> can broaden the parallel current profile. However, when helicity injection is used for startup, relaxation is not required. Startup injection generates a plasma configuration that can be transitioned to inductive or other non-inductive current drive, and closed magnetic flux can be formed transiently without breaking toroidal symmetry. Here, we describe simplified modeling of two HIT-II discharge series that did not produce strong relaxation. Implications of the ‘bubble-burst’ criterion of Ref. 5 for the driven current to expand the injector flux beyond the injector region are reconsidered in terms of the Grad-Shafranov (GS) equation and are used to interpret our results.

Simplified zero- $\beta$  resistive MHD modeling of CHI has been applied to reversed-field pinch, straight tokamak, spheromak, and ST configurations to study magnetic relaxation from current-driven activity.<sup>6-9</sup> All of these studies find that macroscopic symmetry-breaking MHD modes are driven unstable prior to relaxation, but the stabilizing influence of large toroidal field is evident in the tokamak and ST calculations. To obtain information relevant to startup CHI, our

present study applies simplified modeling to conditions in HIT-II discharges that were run without Ohmic drive and did not have strong relaxation.<sup>10</sup> The modeling includes two-dimensional time-dependent MHD computations run to steady state and numerical solution and dimensional scaling of the GS equation. Comparison of the 2D simulation results with relevant data from the HIT-II database shows that the simple model with prescribed diffusion coefficients reproduces the experimentally obtained scaling of plasma current ( $I_p$ ) with external toroidal-field current ( $I_{TF}$ ) and injector flux ( $\psi_{INJ}$ ). After presenting these results, we discuss the connection between the ‘bubble-burst’ and ‘sheet discharge’ analyses in Refs. 5 and 10 with properties of GS solutions.

The zero- $\beta$  model in our time-dependent computations evolves the center-of-mass flow velocity  $\mathbf{V}$  using

$$\rho \left( \frac{\partial}{\partial t} \mathbf{V} + \mathbf{V} \cdot \nabla \mathbf{V} \right) = \mathbf{J} \times \mathbf{B} + \nabla \cdot \rho \nu \left[ \nabla \mathbf{V} + (\nabla \mathbf{V})^T - \frac{2}{3} (\nabla \cdot \mathbf{V}) \mathbf{I} \right] \quad (1)$$

where  $\mathbf{J} = \mu_0^{-1} \nabla \times \mathbf{B}$  is the charge-current density, and  $\nu$  is an isotropic viscous diffusivity. The magnetic field is found from Faraday’s law,  $\partial \mathbf{B} / \partial t = -\nabla \times \mathbf{E}$ , with the resistive-MHD Ohm’s law

$$\mathbf{E} = -\nabla \times \mathbf{B} + \eta \mathbf{J} \quad (2)$$

with resistivity  $\eta$  considered a uniform parameter. The value of  $\eta / \mu_0 = 2.2 \text{ m}^2 / \text{s}$  used in our simulations is based on the 50 eV temperature typically attained in the HIT-II current channel for discharges without strong relaxation. Resistivity is increased by a factor of 30 in a layer along the edge of the computational domain. Evolution of mass density ( $\rho$ ) is not modeled, and the uniform value of  $3.3 \times 10^{-27} \text{ kg/m}^3$  is based on the experimental particle density of  $10^{20} \text{ m}^{-3}$  with deuterium plasma. The viscous diffusivity is set to  $10 \text{ m}^2 / \text{s}$  for numerical purposes.

The time-dependent equations are solved numerically using a subset of the NIMROD implementation.<sup>11</sup> This code has been used for studying helicity injection in spheromaks using boundary conditions that represent either a voltage source<sup>8</sup> or a current source,<sup>12</sup> but the necessity of a downstream absorber<sup>5</sup> requires special consideration for CHI in STs. Specifying voltages across both gaps is problematic on physical grounds, because it presumes knowledge of the rate of change of flux within the domain. Instead, we specify  $RB_\phi$  in excess of the initial vacuum value along the injector gap at the bottom of the domain. The net injected current is then the difference between the  $RB_\phi$ -value specified at the injector gap and its final value along the absorber gap at the top of the domain. At the absorber, we separately specify the voltage (through  $E_R \propto 1/R$ ) and a corresponding outward flow at the  $\mathbf{E} \times \mathbf{B} / B^2$  drift speed to avoid a surface current density. Inflow at the injector is set to match the mass flux at the absorber to avoid large-scale compression or expansion. This approach is effective but not fully satisfactory, because the absorber voltage must be tuned manually. If the applied voltage is too small for a specified  $I_{INJ}$ , it will not support the resistive drop, and the net effect after resistive diffusion includes a change in the actual  $I_{TF}$ . Conversely, applying too much voltage draws poloidal flux into the absorber. In HIT-II, any current that bypassed the plasma discharge by flowing through the shell and across a glow plasma at the absorber was recorded and subtracted from the bank current when determining the net injector current  $I_{INJ}$ .<sup>10</sup> The computational outcome of applying

too little voltage is analogous. The experiment also used a high-capacitance ‘snubber’ across the injector gap to reduce voltage transients, and the current flowing through this capacitor is also excluded from laboratory  $I_{INJ}$  data.

The domain of our computations is a good approximation of the HIT-II cross-section, so that the influence of geometry on the energetics of evolution from a discharge within the injector to an expanded equilibrium in the flux conserver is represented well. The initial poloidal flux distribution (Fig. 1a) approximates the ‘HIT-like,’ i.e. narrow-gap, configuration described in Ref. 10. The HIT-II experiments used active poloidal flux control to maintain equilibrium through times that are longer than the shell diffusion time. Neither resistive-shell nor active control is modeled in the present study; the initial poloidal flux is frozen along the walls. Results from an example time-dependent computation are shown in Fig. 1. The injector flux is  $\psi_{INJ} = 6.5$  mWb, and the applied voltage is increased to 1350 V over 0.1 ms then held constant for 5 ms. During the evolution,  $I_{TF}$  increases from 495 kA to 516 kA, and there is net injection of 9.3 kA in the plasma region. In this case, the applied current of 30 kA is not fully supported by the applied voltage, hence  $I_{INJ}$  is less than the applied values and  $I_{TF}$  drifts by a few percent.

A significant outcome of HIT-II experiments without strong relaxation is that the plasma current obtained in different discharges is approximately independent of  $I_{TF}$ .<sup>10</sup> Obtaining long-lived discharges is aided by the buffering effect of allowing some current to flow through the shell, and the net injected current is then closely tied to the bubble-burst value ( $I_{BB}$ ) that is required to push the injector flux out of its initial distribution. Computed results are plotted in Fig. 2 together with the HIT-II results from narrow-gap discharges with a single-null divertor, discharge series 26449-26476. When performing the computations, we target an  $I_p$ -value by linearly scaling the applied voltage by the nominal  $I_{TF}$  and measure the net  $I_{INJ}$  by subtracting the resulting absorber current from the applied current, analogous to removing the shell current from the experiment’s bank current. The output of the computations is then the net  $I_{INJ}$ , and the trend of  $I_{INJ}$  scaling like  $1/I_{TF}$  is reproduced, at least approximately. Another experimental scan held  $I_{TF}$  at 750 kA while varying  $\psi_{INJ}$  from 2 to 10 mWb. Numerical results are plotted together with the laboratory data from this series, 24954-24971, in Fig. 3. Both experiment and computation show that the plasma current obtained in near-steady profiles depends linearly on  $\psi_{INJ}$ .

As discussed in Ref. 10, the  $I_{TF}$  and  $\psi_{INJ}$  scalings can be related to the injector current required to overcome the vacuum distribution of injector flux, which is concentrated near the injector and extends over the small gap distance  $d$ . The pressure from injected toroidal magnetic field is linearly proportional to  $I_{INJ}$ , because the toroidal-field coil current  $I_{TF}$  is much larger. In contrast, the force that resists expansion depends on  $\psi_{INJ}^2$ . Configurations that do not relax maintain parallel current in the expanded injector flux, producing a toroidal shell or sheet that surrounds the injected toroidal flux.

We observe that the sheet-current model and its conclusions regarding the scaling of  $I_p$  with respect to  $I_{TF}$  and  $\psi_{INJ}$  can be viewed as a dimensional estimate from the GS equation for 2D MHD equilibria,  $\Delta^* \psi = -\mu_0^2 H'$  in the absence of significant plasma pressure. For consistency, we write the equation in terms of physical currents and poloidal flux (no division by  $2\pi$ ),

$\Delta^* \psi = \nabla \cdot (R^{-2} \nabla \psi)$ , and the prime symbol indicates differentiation with respect to  $\psi$ . When there is no significant relaxation, the variation in poloidal flux is tied to the initial injector flux  $\psi_{INJ}$ .

As with all tokamaks,  $I \cong I_{TF}$ , but it varies from  $I_{TF} + I_{INJ}$  to  $I_{TF}$  over  $\Delta\psi = \psi_{INJ}$ . In the vacuum state,  $I' = 0$ , but the external coils force poloidal flux to vary in space over the scale of the injector gap  $d$ . Thus, the injector must raise  $|\mu_0^2 I'| \cong |\mu_0^2 I_{TF} I_{INJ} / \psi_{INJ}|$  to roughly  $|\psi_{INJ}| / d^2$  in order to obtain an appreciable change in the poloidal-flux distribution. From this, one can recognize the bubble-burst criterion from Ref. 5 of  $I_{BB} = K \psi_{INJ}^2 / \mu_0^2 I_{TF} d^2$ , where  $K$  is a dimensionless factor of order unity. Resistive diffusion may influence the width of the current sheet as the injector is applied, but even slow, relatively diffuse evolution can lead to a dramatic change in equilibrium if  $d$  is much smaller than the dimensions of the flux conserver. In the narrow-gap HIT-II discharges,  $d \cong 0.1$  m, so the 5 ms pulse duration allows complete resistive diffusion through the gap length-scale.

After the equilibrium expands into the flux conserver, the width of the current sheet remains at approximately  $d$  to maintain force-balance, based on the GS equation with  $I_{INJ} \cong I_{BB}$ . Since  $\Delta^* \psi = 2\pi\mu_0 R J_T$ , the dimensional estimate predicts  $J_T \cong \psi_{INJ} / 2\pi\mu_0 R d^2$  for the toroidal current density in the sheet. Multiplying  $J_T$  by the cross-section area  $2\pi a d$  of a toroidal shell of radius  $a$  (the minor radius of the flux conserver) then determines  $I_p = \psi_{INJ} a / \mu_0 \bar{R} d$  with a geometrically averaged radius. This relation is tantamount to Eq. (4) and the integration that follows in Ref. 10. It supports the linear scaling of plasma current with respect to  $\psi_{INJ}$  and the finding of  $I_p$  being independent of  $I_{TF}$ . Toroidal geometry affects force-balance and the  $RJ_T$ -value along the inboard part of the current path in HIT-II, where  $d$  is approximately the center-column radius, but among sheet equilibria that expand to fill the flux conserver, these geometric effects are independent of  $I_{TF}$ .

An independent computation for our study solves the GS equation numerically with an assumed  $I(\psi)$  profile. We apply the NIMEQ solver<sup>13</sup> that uses NIMROD's meshing and spectral finite elements, and we incorporate the same geometry and injector-flux distribution that have been considered with the time-dependent computations. Three equilibria computed from the vacuum-flux distribution with  $\psi_{INJ} = 6.5$  mWb of Fig. 1a and  $I_{TF} = 500$  kA are shown in Fig. 4. The assumed current distribution is

$$I(\tilde{\psi}) = I_{TF} + 0.5I_{INJ} - 0.5I_{INJ} \tanh(\tilde{\psi}) \quad , \quad (3)$$

where the normalized  $\tilde{\psi} \cong 2(1000\psi / \pi - 0.7)$  for  $\psi$  in mWb. With  $d = 0.1$  m and  $K$  set to unity, the approximate criterion for bubble burst in these conditions is  $\psi_{INJ}^2 / \mu_0^2 I_{TF} d^2 = 5.4$  kA. Figures 4a-b show the poloidal flux and current distributions with a relatively small injector current of  $I_{INJ} = 2.5$  kA specified in Eq. (3). More than half of the poloidal flux contours remain in the injector, and a significant amount of closed poloidal current flows within the flux conserver. This state is therefore not sustainable without relaxation or Ohmic current drive. The second result, shown in Figs. 4c-d, has  $I_{INJ} = 5$  kA specified. A larger fraction of the poloidal flux is open, so it is a better representation of weakly relaxing conditions; though, the poloidal flux value in the flux conserver exceeds the specified injector range by 6%. The result of Figs. 4d-e has  $I_{INJ} = 10$  kA specified in the GS computation, and the poloidal flux in the flux conserver exceeds the injector range by a somewhat more substantial 17%. While non-relaxing dynamics cannot produce this amplification, both larger- $I_{INJ}$  equilibria display sheet-like  $I(\psi)$  profiles with

variation over the injector-gap scale. These GS solutions are close to the  $I_{TF} = 500$  kA results from experiment and time-dependent computations; the injected 5 kA and 10 kA values and the resulting  $I_p$ -values of 71 kA and 119 kA bracket the  $I_{TF} = 500$  kA results in Fig. 2. The GS solution with  $I_{INJ} = 2.5$  kA produces only 34 kA of plasma current, while another case with  $I_{INJ} = 20$  kA produces 188 kA of plasma current and 27% flux amplification. This represents a qualitatively significant change in the equilibrium state as  $I_{INJ}$  is varied over the bubble-burst estimate.

Our comparisons show that time-dependent computations from a basic resistive-MHD model reproduce important scalings of HIT-II in discharges powered by CHI alone. We emphasize the connection between the modeling in Ref. 10 with dimensional estimates from the GS equation and note that the bubble-burst condition represents a transition among equilibria as the injector current is varied. Computing GS solutions with an assumed  $I(\psi)$  profile shows the transition at injector-current values that are consistent with the experimental results and the time-dependent computations; though, some aspects of our GS solutions are not dynamically attainable. The time-dependent computations with a simple resistive-MHD Ohm's law and a fixed value of resistivity are more reliable in this regard.

Three-dimensional time-dependent computations have been used to check some of the parameters considered here. Like the HIT-II results from these discharge series, no significant relaxation is observed. Other 3D computations with smaller  $I_{TF}$  produce significant relaxation and flux amplification. More detailed modeling including energy transport and 3D relaxation is presently being applied to model CHI in the NSTX experiment.<sup>14</sup>

This work is supported by the U. S. Department of Energy grant DE-FC02-05ER54813 as part of the Plasma Science and Innovation Center. Computations have been performed at the National Energy Research Scientific Computing Center, which is supported by the Office of Science of the U. S. Dept. of Energy under Contract No. DE-AC02-05CH11231.

<sup>1</sup>T. H. Jensen and M. S. Chu, Phys. Fluids **27**, 2881 (1984).

<sup>2</sup>T. R. Jarboe, M. A. Bohnet, A. T. Mattick, B. A. Nelson, and D. J. Orvis, Phys. Plasmas **5**, 1807 (1998).

<sup>3</sup>A. J. Redd, B. A. Nelson, T. R. Jarboe, P. Gu, R. Raman, R. J. Smith, and K. J. McCollam, Phys. Plasmas **9**, 2006 (2002).

<sup>4</sup>J. B. Taylor, Phys. Rev. Lett. **33**, 1139 (1974).

<sup>5</sup>T. R. Jarboe, Fusion Technology **15**, 7 (1989).

<sup>6</sup>Y. L. Ho, Nucl. Fusion **31**, 341 (1991).

<sup>7</sup>C. R. Sovinec and S. C. Prager, Phys. Plasmas **3**, 1038 (1996).

<sup>8</sup>C. R. Sovinec, J. M. Finn, and D. del-Castillo-Negrete, Phys. Plasmas **8**, 475 (2001).

<sup>9</sup>X. Z. Tang and A. H. Boozer, Phys. Plasmas **11**, 2679 (2004).

<sup>10</sup>A. J. Redd, T. R. Jarboe, B. A. Nelson, R. G. O'Neill, and R. J. Smith, Phys. Plasmas **14**, 112511 (2007).

<sup>11</sup>C. R. Sovinec, A. H. Glasser, T. A. Gianakon, *et al.*, J. Comput. Phys. **195**, 355 (2004).

<sup>12</sup>B. I. Cohen, E. B. Hooper, R. H. Cohen, D. N. Hill, H. S. McLean, R. D. Wood, S. Woodruff, C. R. Sovinec, and G. A. Cone, Phys. Plasmas **12**, 56106 (2005).

- <sup>13</sup>E. C. Howell and C. R. Sovinec, Bull. Am. Phys. Soc. **53**, No. 14, BAPS.2008.DPP.BP6.41 (2008).
- <sup>14</sup>E. B. Hooper, R. Raman, J. E. Menard, and C. R. Sovinec, Bull. Am. Phys. Soc. **55**, No. 15, BAPS.2010.DPP.BP9.71 (2010).

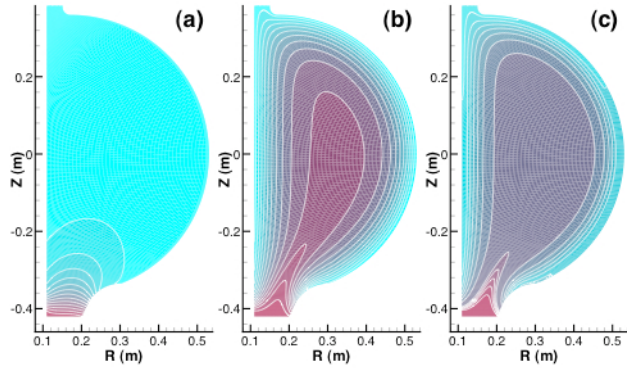


Figure 1. (Color online) Contours of (a) initial poloidal flux, (b) final poloidal flux, and (c) final  $RB_\phi$  from a time-dependent NIMROD computation run to steady state with  $\psi_{INJ} = 6.5$  mWb and 9.3 kA of net current injected into the computational domain.

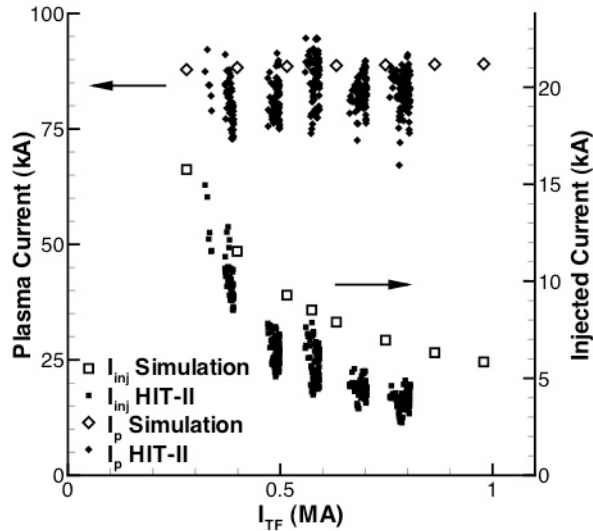


Figure 2. Net injected current and plasma current as external toroidal-field current is varied. Results are from NIMROD simulations run to steady state and from the HIT-II discharge series 26449-26476.

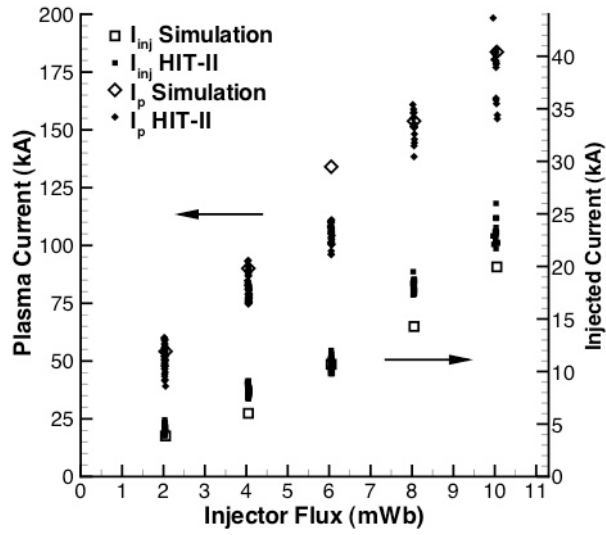


Figure 3. Net injected current and plasma current as injector flux is varied. Results are from NIMROD simulations run to steady state and from the HIT-II discharge series 24954-24971.

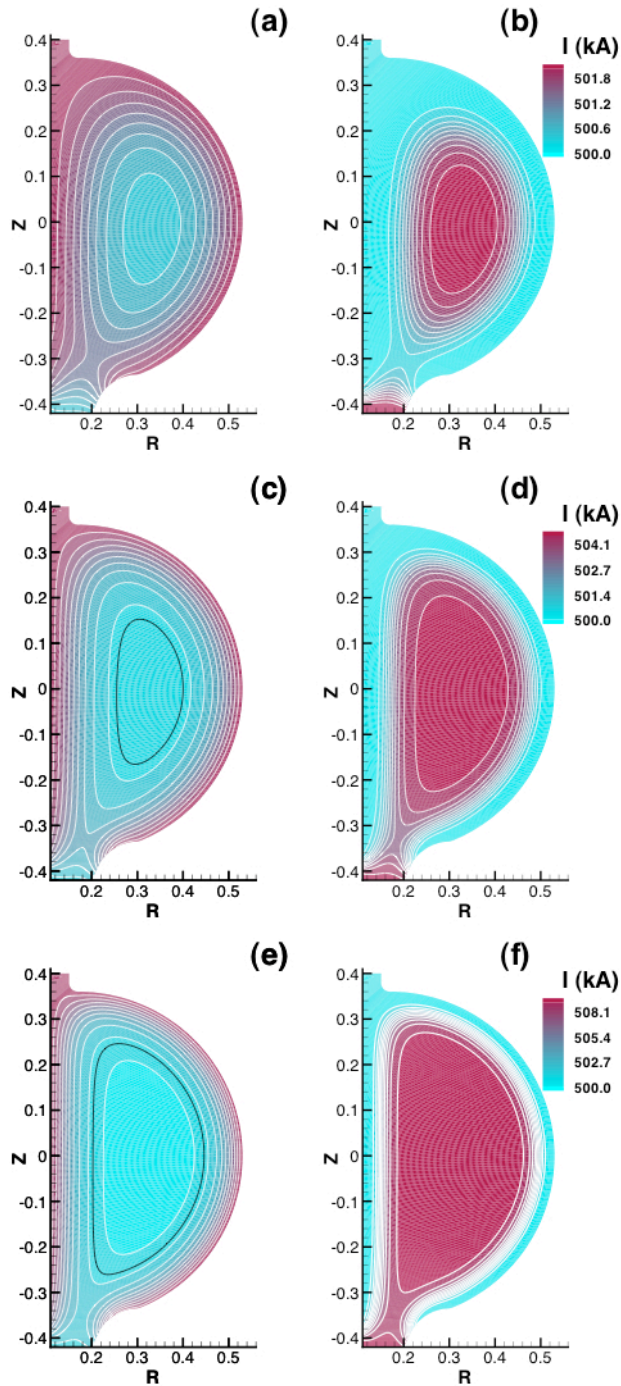


Figure 4. (Color online) Results of GS computations with the hyperbolic-tangent  $I(\psi)$  profile given in Eq. (3) with  $I_{TF} = 500$  kA,  $\psi_{INJ} = 6.5$  mWb and varying injector current. Frames (a-b) show poloidal flux and poloidal current, respectively, for  $I_{INJ} = 2.5$  kA, frames (c-d) are for  $I_{INJ} = 5$  kA, and frames (e-f) are for  $I_{INJ} = 10$  kA. The white contour lines in the flux plots are evenly spaced from  $-1.13$  mWb to  $6.48$  mWb, and the black contour in (c) and (e) indicates the lower limit of the injector flux,  $\psi = 0$ .